

Supporting Information

Binding sites-driving sensing properties of a quinazoline derivative with metal cations

Yang Liu, Dan Wang, Xiang-Jun Zheng*, Lin-Pei Jin

Beijing Key Laboratory of Energy Conversion and Storage Materials, College of Chemistry, Beijing Normal University, Beijing, 100875, People's Republic of China

**Corresponding author email: xjzheng@bnu.edu.cn*

Table S1 Selected Bond Distances (Å) and Angles (deg) for **1** and **2**.

1					
Cd(1)-O(1)	2.586(9)	Cd(1)-O(2)	2.217(8)	Cd(1)-O(3)	2.594(6)
Cd(1)-O(4)	2.295(9)	Cd(1)-N(3)	2.295(9)	Cd(1)-N(5)	2.333(7)
O(1)-Cd(1)-O(2)	53.3(3)	O(1)-Cd(1)-O(3)	82.26(11)	O(1)-Cd(1)-O(4)	97.9(3)
O(1)-Cd(1)-N(3)	94.7(3)	O(1)-Cd(1)-N(5)	158.8(3)	O(2)-Cd(1)-O(3)	96.6(3)
O(2)-Cd(1)-O(4)	143.67(12)	O(2)-Cd(1)-N(3)	98.9(3)	O(2)-Cd(1)-N(5)	106.0(3)
O(3)-Cd(1)-O(4)	53.6(3)	O(3)-Cd(1)-N(3)	158.1(3)	O(3)-Cd(1)-N(5)	97.0(3)
O(4)-Cd(1)-N(3)	105.9(3)	O(4)-Cd(1)-N(5)	98.6(3)	N(3)-Cd(1)-N(5)	93.50(11)

2					
Cd(1)-N(2)	2.329(16)	Cd(1)-N(4)	2.199(14)	Cd(1)-Cl(2)	2.430(5)
Cd(1)-Cl(3)	2.421(6)	N(2)-Cd(1)-Cl(2)	106.6(4)	N(2)-Cd(1)-Cl(3)	118.8(4)
N(2)-Cd(1)-N(4)	96.5(2)	N(4)-Cd(1)-Cl(2)	119.0(4)	N(4)-Cd(1)-Cl(3)	108.3(4)
Cl(3)-Cd(1)-Cl(2)	107.93(8)				

Table S2 Comparison of the chemosensors for Al³⁺, Cr³⁺ and Fe³⁺ ions

Chemosensor	Detected cation	Detection limit	Differentiation of one from another	Reference
Chromo-fluorogenic probe	Al ³⁺ , Cr ³⁺ , Fe ³⁺	10 ⁻⁸ M	√	8a
Pyridinyl-functionalized tetraphenylethene	Al ³⁺ , Cr ³⁺ , Fe ³⁺	10 ⁻⁶ M		8b
Spirobenzopyran-quinoline dyad	Al ³⁺ , Cr ³⁺ , Fe ³⁺	10 ⁻⁶ M	√	8c
ESIPT based sensor	Al ³⁺ , Cr ³⁺ , Fe ³⁺	10 ⁻⁶ M		8d
Chemodosimetric probe	Al ³⁺ , Cr ³⁺ , Fe ³⁺	10 ⁻⁸ M		8g
RhB-based probe	Al ³⁺ , Cr ³⁺ , Fe ³⁺	10 ⁻⁵ -10 ⁻⁷ M		8e
Rhodamine-naphthalimide dyad	Al ³⁺ , Cr ³⁺ , Fe ³⁺	10 ⁻⁵ M		8f
6-furan-2-yl-5,6-dihydrobenzo(4,5)imidazo[1,2-c]quinazoline	Al ³⁺ , Cr ³⁺ , Fe ³⁺	10 ⁻⁶ M	√	Our paper

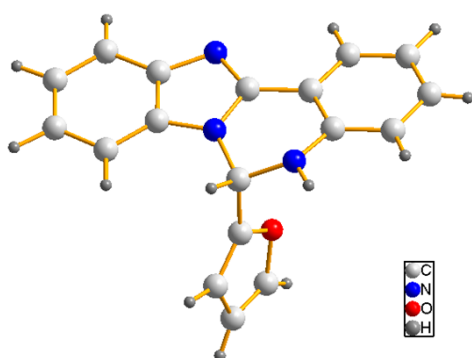


Figure S1 Crystal structure of L.

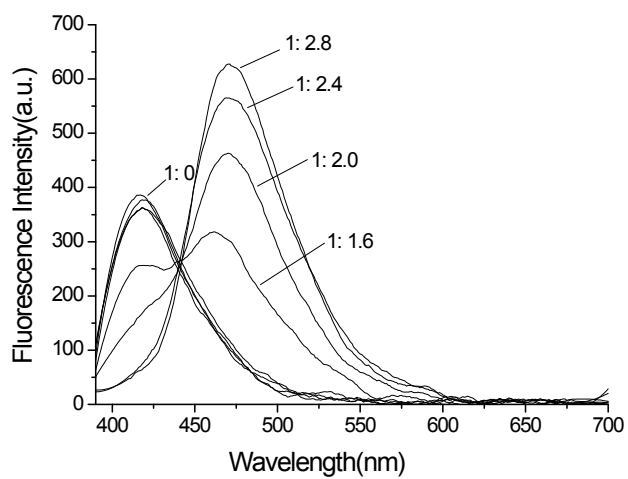


Figure S2 Fluorescence properties of L (100 μ M) in CH_3OH with HCl (0, 0.4, 0.8, 1.2, 1.6, 2.0, 2.4, 2.8 equiv.)

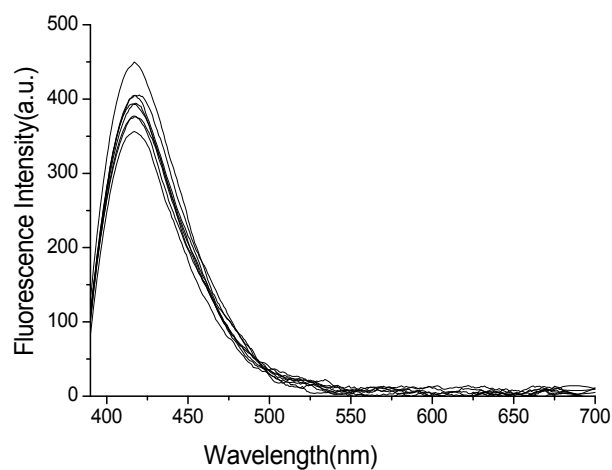
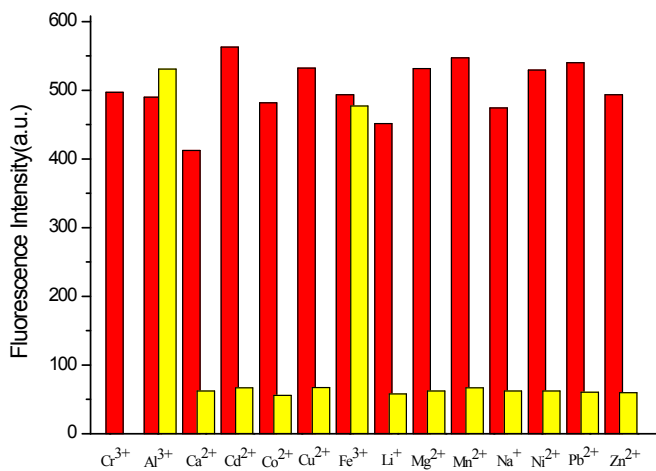
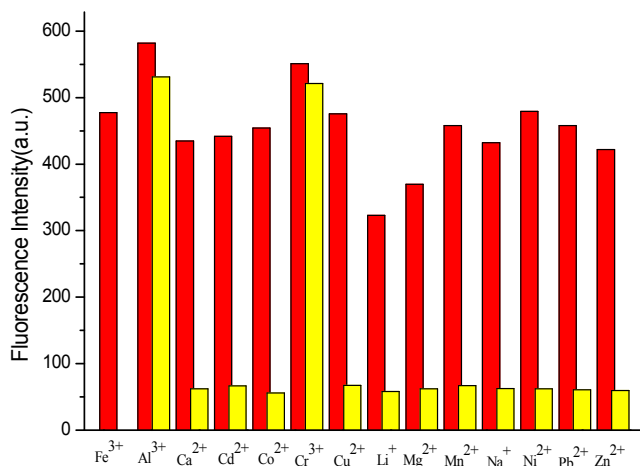


Figure S3 Fluorescence properties of L (100 μ M) in CH_3OH with NaOH (0, 0.4, 0.8, 1.2, 1.6, 2.0, 2.4, 2.8 equiv.)

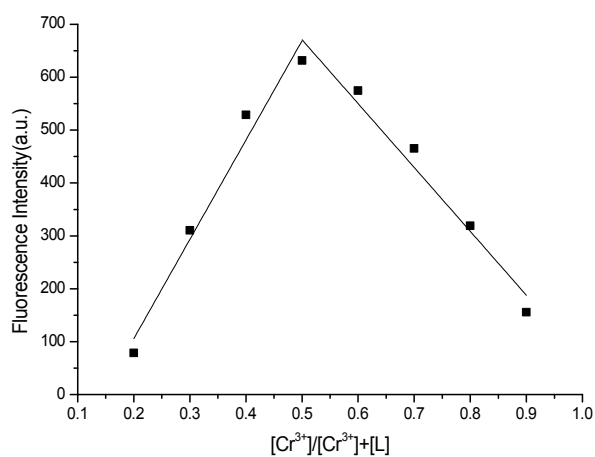


(a)

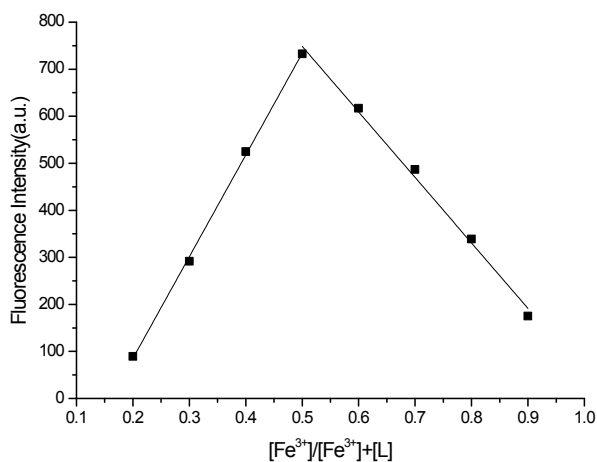


(b)

Figure S4 (a) Fluorescence intensity of complexes of L and Cr^{3+} in the presence of various metal ions in CH_3OH . $\lambda_{\text{ex}}=390$ nm and $\lambda_{\text{em}}=471$ nm. Red bars: L($30\mu\text{M}$) with 1.0 equiv. of Cr^{3+} and 1.0 equiv. of other metal ions stated. Yellow bars: L($30\mu\text{M}$) with 1.0 equiv. of other metal ions stated; (b) Fluorescence intensity of complexes of L and Fe^{3+} in the presence of various metal ions in CH_3OH . $\lambda_{\text{ex}}=388$ nm and $\lambda_{\text{em}}=470$ nm. Red bars: L($30\mu\text{M}$) with 1.0 equiv. of Fe^{3+} and 1.0 equiv. of other metal ions stated. Yellow bars: L($30\mu\text{M}$) with 1.0 equiv. of other metal ions stated.

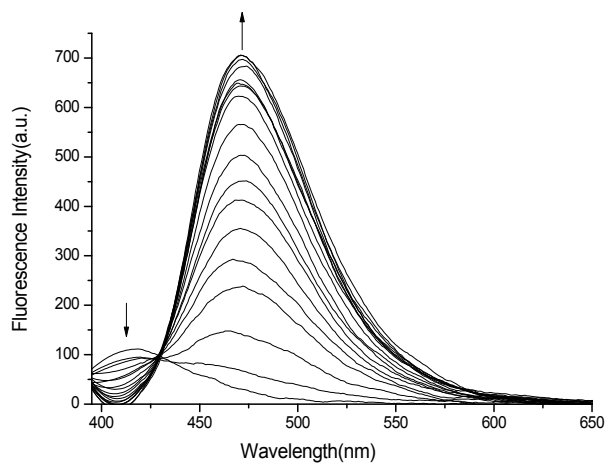


(a)

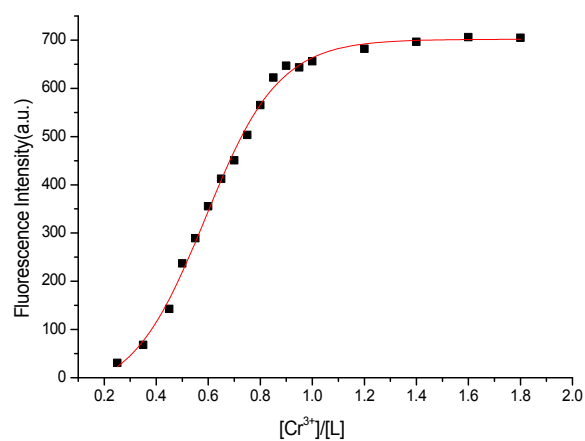


(b)

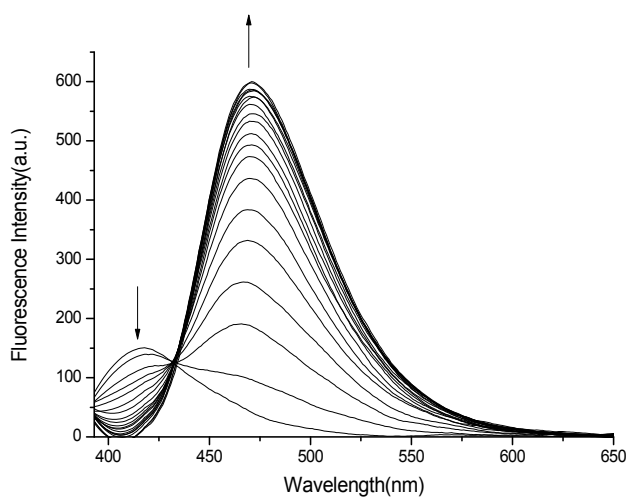
Figure S5 (a) Job's plot for the determination of the stoichiometry of L and Cr^{3+} in the complexation; (b) Job's plot for the determination of the stoichiometry of L and Fe^{3+} in the complexation.



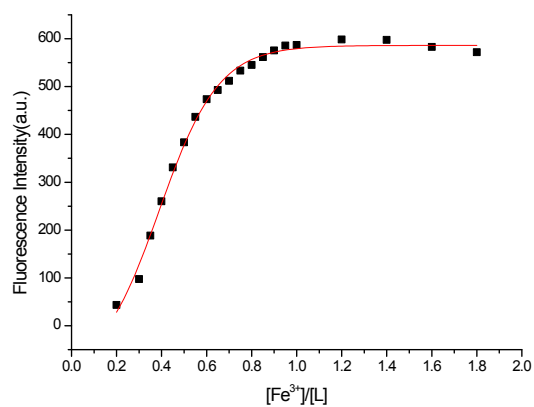
(a)



(b)

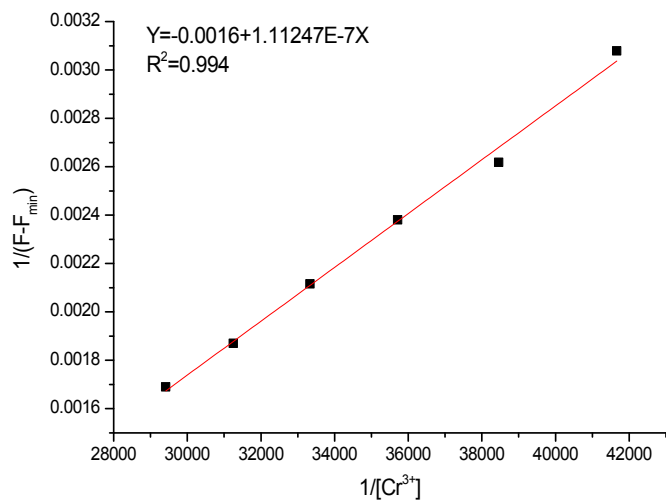


(c)

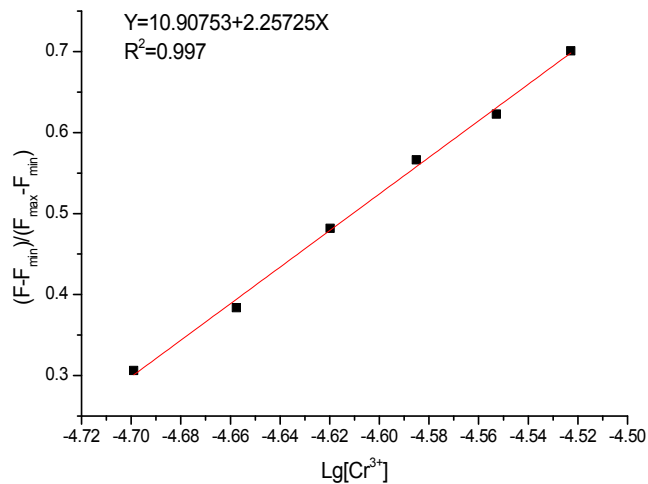


(d)

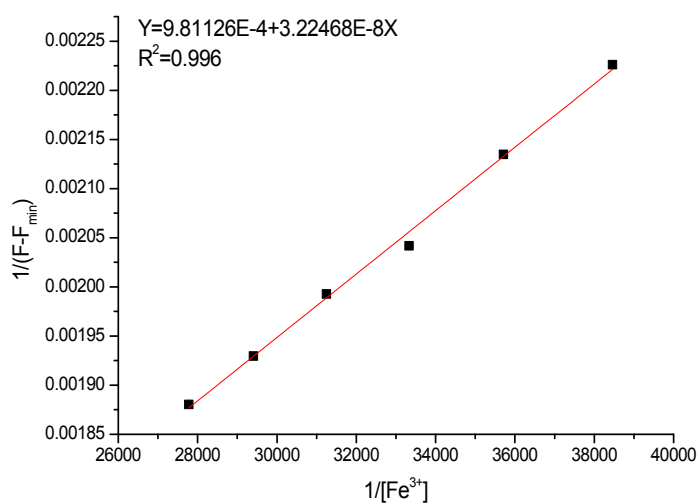
Figure S6 (a) Fluorescence emission spectra($\lambda_{\text{ex}}=390\text{nm}$) of L($40\mu\text{M}$) in the presence of increasing amounts of Cr^{3+} (0.25, 0.35, 0.45, 0.50...0.80, 0.85, 0.90, 0.95, 1.00, 1.20, 1.40, 1.60, 1.80 equiv.) in CH_3OH ; (b) Spectrofluorimetric titration curve at $\lambda_{\text{em}}=471\text{nm}$; (c) Fluorescence emission spectra($\lambda_{\text{ex}}=388\text{nm}$) of L($40\mu\text{M}$) in the presence of increasing amounts of Fe^{3+} (0.20, 0.30, 0.35, 0.45, 0.50...0.80, 0.85, 0.90, 0.95, 1.00, 1.20, 1.40, 1.60, 1.80 equiv.) in CH_3OH ; (d) Spectrofluorimetric titration curve at $\lambda_{\text{em}}=471\text{nm}$.



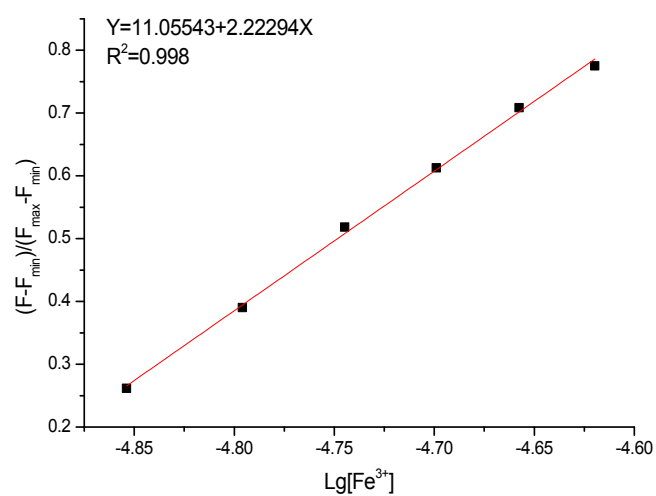
(a)



(b)



(c)



(d)

Figure S7 (a) Benesi-Hildebrand plot of L with Cr³⁺ in CH₃OH (λ_{em} = 471 nm); (b) Normalized response of emission signal changing Cr³⁺ concentrations at 471 nm; (c) Benesi-Hildebrand plot of L with Fe³⁺ in CH₃OH (λ_{em} = 470 nm); (d) Normalized response of emission signal changing Fe³⁺ concentrations at 470 nm.

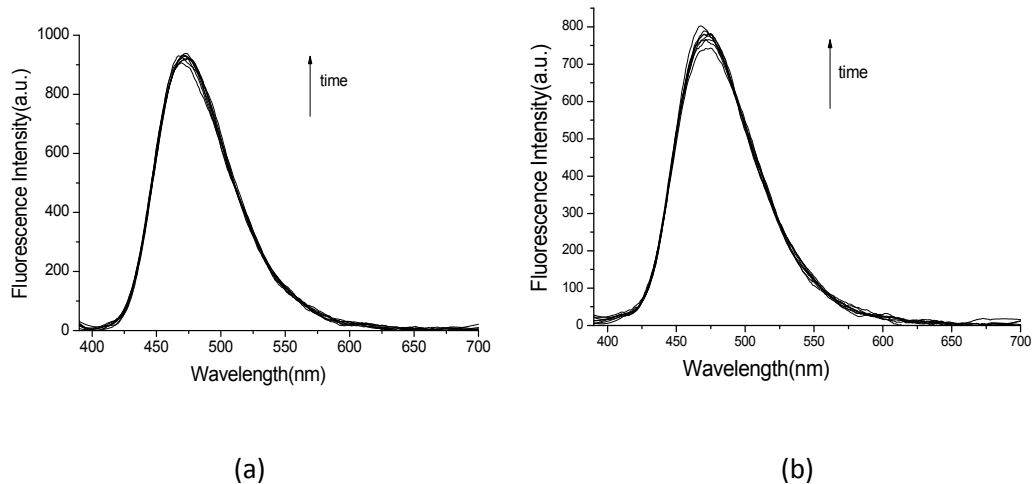


Figure S8 Fluorescence spectra variation of L (67 μM) upon addition of 1.0 equiv. of Al^{3+} (a) and Fe^{3+} (b) in CH_3OH after 1, 2, 3, 4, 5, 10, 15, and 20 min, $\lambda_{\text{ex}}=383$ nm.

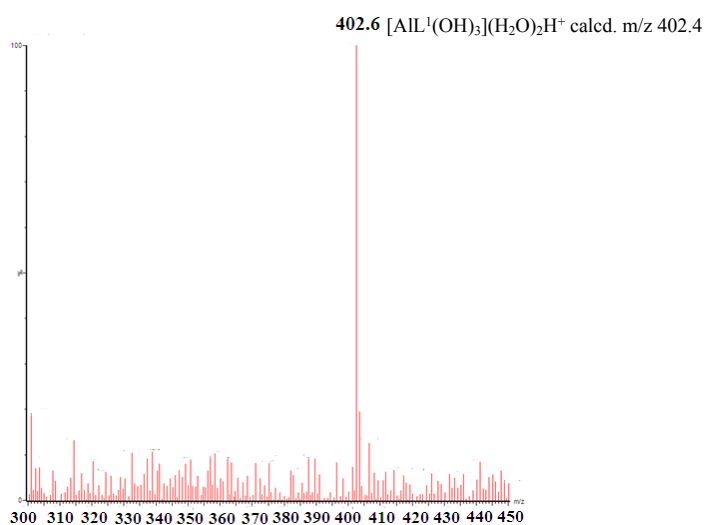


Figure S9 ESI-MS of $\text{L-Al}^{3+}(1:1)$ in $\text{CH}_3\text{OH}/\text{H}_2\text{O}$ (1:9).

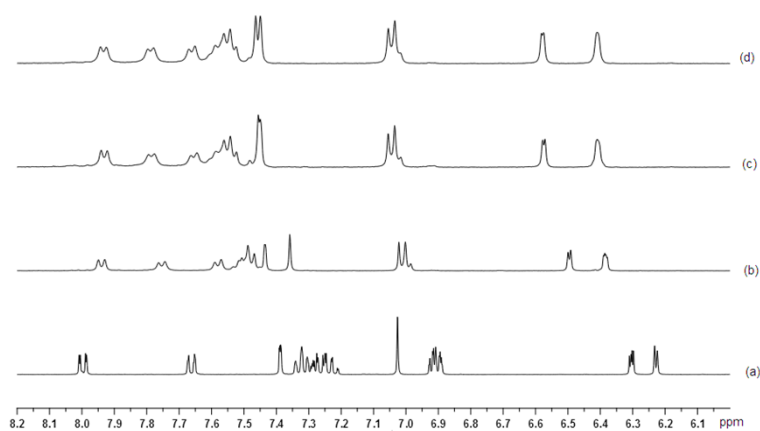


Figure S10 ^1H NMR spectra in $\text{CH}_3\text{OH-d}_6$: (a) L only; (b) L and 0.5 equiv. of Cr^{3+} ; (c) L and 1.0 equiv. of Cr^{3+} ; (d) L and 1.5 equiv. of Cr^{3+} .

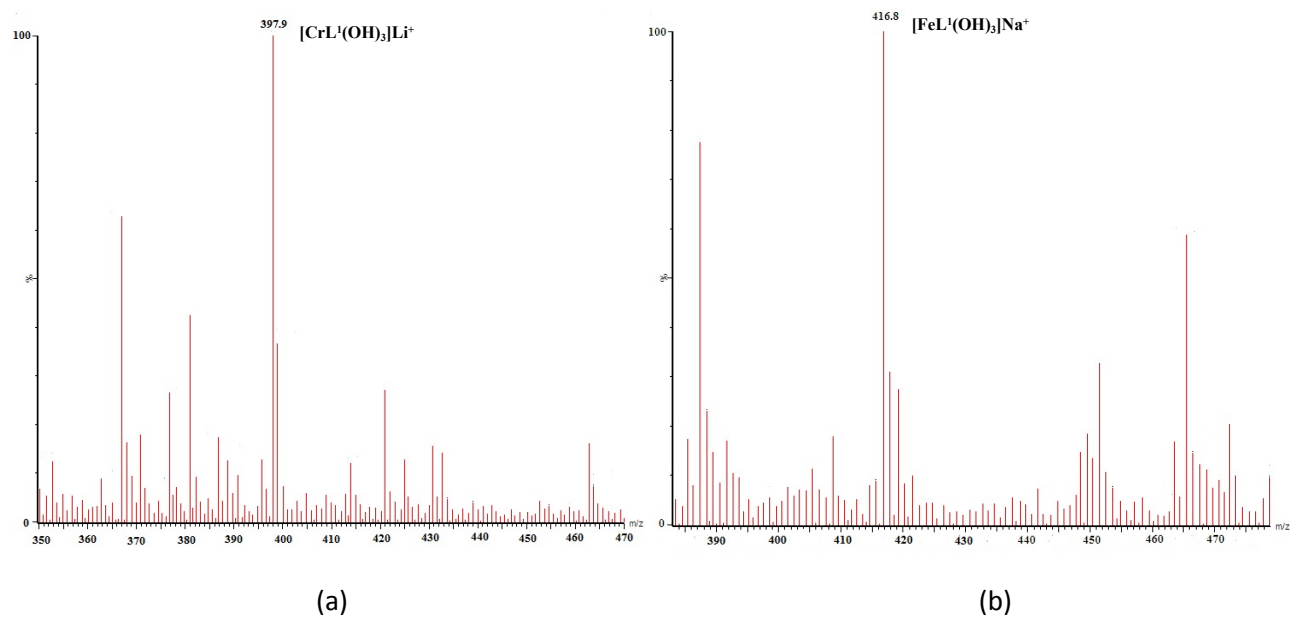


Figure S11 (a) Positive-ion electrospray ionization mass spectra of L upon addition of 1.0 equiv. Cr^{3+} in CH_3OH ; (b) Positive-ion electrospray ionization mass spectra of L upon addition of 1.0 equiv. Fe^{3+} in CH_3OH .

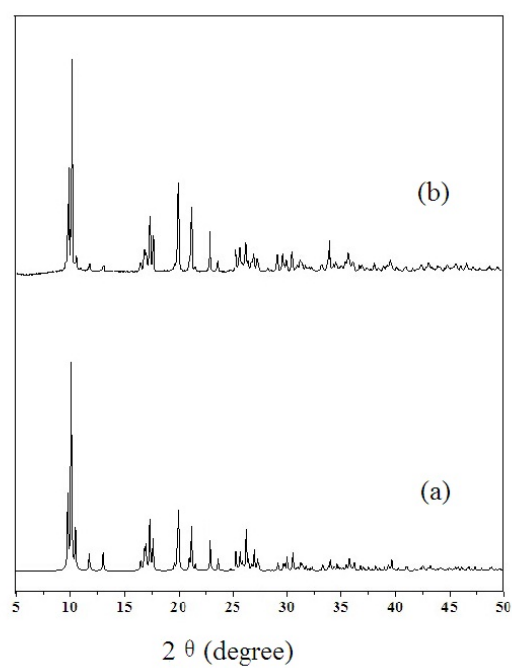


Figure S12 (a) Simulated Powder X-ray diffraction for $[\text{CdL}_2(\text{OAc})_2]$; (b) Powder X-ray diffraction for sample **1'**.

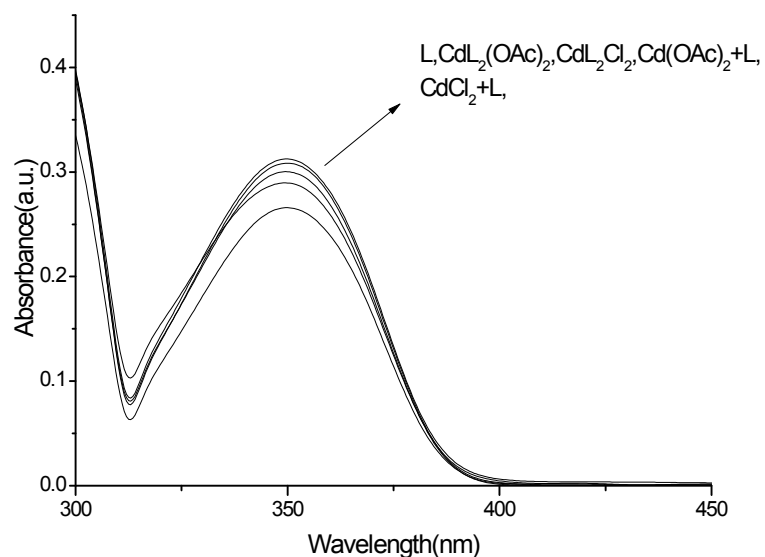


Figure S13 UV-Vis absorptionspectra of CdL₂(OAc)₂(15 μM), CdL₂Cl₂(15 μM), L(30 μM) and L(30 μM) with 1.0 equiv. of CdCl₂, Cd(OAc)₂ in CH₃OH, respectively.

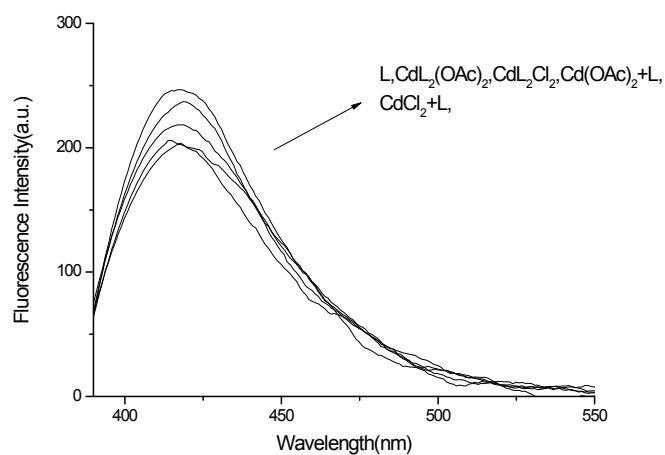


Figure S14 Fluorescence spectra of CdL₂(OAc)₂(15 μM), CdL₂Cl₂(15 μM), L(30 μM) , and L(30 μM) with 1.0 equiv. of CdCl₂, Cd(OAc)₂ in CH₃OH, respectively.

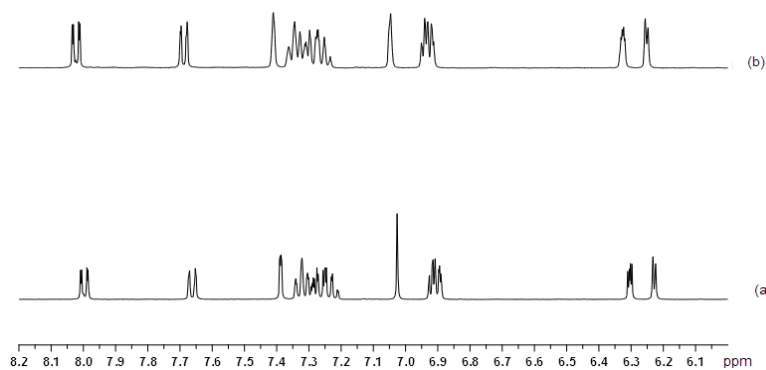


Figure S15 ¹H NMR spectra in CH₃OH-d₆: (a) L; (b) CdL₂(OAc)₂.